Submitted to ADVANCED MATERIALS

DOI: 10.1002/adma.((please add manuscript number))

Fabrics with Tunable Oleophobicity

By *Wonjae Choi*,[1**] *Anish Tuteja*,[2**] *Shreerang Chhatre*,[2] *Joseph M. Mabry*,[3] *Robert E. Cohen*[2]* and *Gareth H. McKinley*[1]*

([**]: these authors contributed equally to this work)

[1] Prof. Gareth H. McKinley, Wonjae Choi
Department of Mechanical Engineering, Massachusetts Institute of Technology
Cambridge, MA 02139 (USA)

[2] Prof. Robert E. Cohen, Dr. Anish Tuteja, Shreerang Chhatre
Department of Chemical Engineering, Massachusetts Institute of Technology
Cambridge, MA 02139 (USA)

[3] Dr. Joseph M. Mabry
Space and Missile Propulsion Division, Air Force Research Laboratory
Edwards Air Force Base, CA 93524 (USA)

*: Corresponding authors
Prof. Gareth H. McKinley (gareth@mit.edu)
Prof. Robert E. Cohen (recohen@mit.edu)

Acknowledgement. This research has been supported by the Air Force Research Lab (AFRL) under contract no. FA9300-06M-T015 and the Air Force Office of Scientific Research (AFOSR) under contract no. FA9550-07-1-0272 and LRIR-92PL0COR. We also thank Prof. Michael F. Rubner and the Institute for Soldier Nanotechnologies (ISN) at MIT for the use of various lab facilities. Partial financial support for S.C. starting Sept. 1, 2008 was provided by the Army Research Office (ARO) through contract no. W911NF-07-D-0004.

Keywords: Superoleophobic, Super-wetting, Super-repellency, Dip-coating, Tunable wettability

Extreme wetting behavior, *super-repellency* and *super-wetting*, has recently generated immense commercial and academic interest[1-10] due to its wide applicability in various fields including the development of self-cleaning surfaces,[11] liquid-liquid separation membranes,[12] and anti-fogging films.[13] Various research groups have also tried to develop surfaces that can effectively switch their surface wetting properties in response to changes in their surrounding environment.[14] This includes surfaces that alter their wettability in response to changes in temperature,[8] electrical voltage[15, 16] and mechanical deformation.[17, 18] Because of the difficulty of making surfaces that are strongly repellent to low surface tension liquids such as oils and alcohols, most work on switchable wettability has focused on studies with water droplets[10] (with the exception of recent work of Ahuja et al.[15]). In our previous work we have demonstrated how the incorporation of re-entrant surface texture, (i.e. a multi-valued surface topography) in conjunction with surface chemistry can be used to fabricate superoleophobic surfaces, i.e. surfaces which can support a robust composite (solid-liquid-air) interface and display contact angles greater than 150° with various low surface tension liquids.[19] More recently, we have also developed two general design parameters that can aid the systematic design of omniphobic surfaces that resist wetting by almost any liquid.[20]

In the present work, we analyze the consequences of these non-wetting design parameters more extensively. Recognizing the role of re-entrant surface features, we first develop a simple dip-coating process for delivering a conformal coating of fluorodecyl POSS molecules.[19, 21] This coating enables us to bestow substantially enhanced liquid repellency to any substrate already possessing suitable textures, such as the lotus leaf, commercial fabrics and even duck feathers, by promoting the formation of a composite (solid-liquid-air) interface. Consideration of the geometric scaling of the design parameters suggests that mechanically deforming a re-entrant structure such as a dip-coated commercial fabric will lead to a dramatic, but reversible, reduction in the liquid repellency of the surface. Indeed, we observe that a non-

wetting drop (initially sitting on the surface in a composite Cassie-Baxter state) completely wets into the fabric texture beyond a critical imposed strain, leading to near zero contact angles. This allows us to develop, for the first time, surfaces that exhibit reversible, deformation-dependent, tunable wettability, including the capacity to switch their surface wetting properties (between super-repellent and super-wetting) against a wide range of polar and non-polar liquids.

When a liquid contacts a textured surface, such as the one shown in **Fig. 1a**, then, provided the pressure difference across the liquid-air interface is negligible, the liquid does not penetrate fully into the pores of the surface texture. Instead, the liquid wets the pore surface partially until the local angle (ψ) between the liquid and the textured substrate becomes equal to the equilibrium contact angle θ (given by Young's relation[22]) for the three phase contact line.[23-25] The existence of points on the surface that enables the condition $\psi = \theta$ [26] to be fulfilled is a necessary, though not sufficient condition,[19, 24, 25, 27, 28] for the formation of a composite interface, such as the one shown in Fig. 1a.

The apparent contact angle θ^* for the composite interface that exists under a strongly non-wetting droplet is typically computed using the Cassie-Baxter relation:

$$\cos\theta^* = f_1 \cos\theta + f_2 \cos\pi = f_1 \cos\theta - f_2 \qquad (1)$$

where f_1 is the ratio of the total area of solid-liquid interface to a unit projected area of the textured substrate and f_2 is the corresponding ratio for the liquid-air interface.[23] An example of a natural surface that is able to support a composite interface is shown in Fig. 1b, which illustrates water (γ_v = 72.1 mN/m) droplets 'beading up' on the surface of a duck feather. The feather is composed of a periodic array of micron-scale cylindrical barbules (see SEM in supporting information). The bright, reflective surface visible underneath the water droplet in Fig. 1b is a signature of trapped air and the establishment of a composite solid-liquid-air interface. The formation of this 'Cassie-Baxter' state enhances super-repellency by promoting

a high apparent contact angle (θ^*) and low contact angle hysteresis (defined as the difference between the advancing and receding contact angles) when $f_1 << 1$.[23, 29-32]

On the other hand, if the liquid fully penetrates into the texture surface, then the apparent contact angle θ^* is determined by the Wenzel relation:[33]

$$\cos\theta^* = r\cos\theta \qquad (2)$$

where r is the surface roughness, defined as the ratio between the actual surface area and the projected area. Since r is necessarily greater than unity, roughness amplifies both the wetting and non-wetting behavior of materials in the Wenzel regime; i.e. $\cos\theta^* >> 0$ if $\cos\theta > 0$ and $\cos\theta^* << 0$ if $\cos\theta < 0$. A consequence of this dependence on the roughness of the texture is that, once initiated, the imbibition of a liquid drop into a roughened texture can rapidly lead to super-wetting because the apparent contact angle $\theta^* \rightarrow 0°$ when $r >> 1$ and $\theta < 90°$.

Development of extremely liquid-repellent surfaces requires the design of substrates that promote the formation of a composite interface with any liquid. The two important design characteristics for establishing a composite 'Cassie-Baxter' state on a textured surface with a particular contacting liquid are (i) the magnitude of the apparent contact angle θ^* on the composite interface and (ii) the robustness of the composite interface against external perturbation. The equilibrium apparent contact angles on the texture can be readily estimated using the Cassie-Baxter relation (Eq. 1), and in our recent work we developed a dimensionless design parameter A^* to predict the robustness of the composite interface.[20] This robustness factor represents the ratio between the breakthrough pressure required to cause sufficient sagging and disruption of the liquid-vapor interface (see Fig. 1c), and a characteristic reference pressure P_{ref}, given as $P_{ref} = 2\gamma_{lv}/\ell_{cap}$, where $\ell_{cap} = \sqrt{\gamma_{lv}/\rho g}$ (here ρ is the fluid density and g is the acceleration due to gravity). This reference pressure P_{ref} is close to the minimum pressure difference across the composite interface for millimetric or larger liquid

droplets or puddles,[20] and the breakthrough pressure at which a given composite interface is disrupted can be computed as $P_{breakthrough} \approx A^* \times P_{ref}$.

For a texture that is dominated by periodic cylindrical features, such as the duck feathers shown in Fig. 1 and the fabric surface shown in **Fig. 3**, the robustness measure A^* can be calculated to be (see supporting information):

$$A^* = \frac{P_{breakthrough}}{P_{ref}} = \frac{R\ell_{cap}}{D^2} \frac{(1-\cos\theta)}{(1+2(R/D)\sin\theta)} \quad (3)$$

Here R is the fiber radius and D is half the inter-fiber gap, as shown in Fig. 1a. Large values of the robustness factor ($A^* >> 1$) indicate the formation of a robust composite interface, with very high breakthrough pressures. On the other hand, as A^* approaches unity, $P_{breakthrough}$ decreases towards P_{ref}. Thus, a composite interface on any surface for which $A^* < 1$ cannot maintain its stability against even small pressure differentials across the liquid-air interface, causing the liquid to penetrate into the textured surface and ultimately to be fully imbibed.

It is also useful to define another dimensionless parameter, D^*, that parameterizes the geometry of the re-entrant features. For a texture consisting of uniform cylindrical features as shown in Fig. 1a, the ratios f_1 and f_2 in the Cassie–Baxter relationship[23] (Eq. 1) become $f_1 = R(\pi-\theta)/(R+D)$ and $f_2 = 1 - R\sin\theta/(R+D)$. Substituting these expressions into Eq. 1 and factoring out a dimensionless spacing ratio $D^* = (R+D)/R$ enables us to express the apparent contact angle in terms of a purely geometric factor and a contribution involving the equilibrium contact angle on a flat surface:

$$\cos\theta^* = -1 + \frac{1}{D^*}\left[\sin\theta + (\pi-\theta)\cos\theta\right] \quad (4)$$

Higher values of D^* correspond to a higher fraction of air in the composite interface (f_2 in Eq. 1), and consequently an increase in the apparent contact angle θ^* for a given liquid. Care must be taken in developing appropriate expressions for D^* and A^* for surfaces with variable

surface texture parameters or multiple scales of roughness such as a duck feather or a lotus leaf (see supporting information for further details).[34, 35]

To achieve high apparent contact angles with low contact angle hysteresis and a robust composite interface, we seek to maximize the two design parameters D^* and A^* simultaneously. However, for a periodic geometry of cylindrical features, these two design factors are strongly coupled. Increasing the value of D^*, by either increasing D or reducing R (with the other geometric variable held fixed), leads to a decrease in the values of A^* (see Eq. 3). This coupling is further highlighted in **Fig. 2** which shows a general design chart for a typical oil (rapeseed oil; γ_{lv} = 35.7 mN/m, $\theta = 86^o$) on a surface with cylindrical fibers, illustrating the variation in the robustness factor A^* with the variation in the spacing ratio D^*. The solid lines in the graph correspond to A^* values computed by changing the inter-fiber distance (D) while maintaining the fiber radius (R) constant. Each solid line corresponds to a different value of the fiber radius R, varying between 1 mm – 1 nm.

Evaluating the magnitude of the robustness factor A^* also explains why rapeseed oil spontaneously penetrates the texture of many naturally re-entrant superhydrophobic surfaces such as a duck feather or a lotus leaf (see inset of **Fig. 3a**, $D^* \approx 58$; also see supporting information). In each case, $A^* << 1$ as shown in Fig. 2. To enable these surfaces to support a composite interface with various low surface tension liquids, it is essential to increase the magnitude of the robustness factor A^*. For a fixed surface texture, such an enhancement can be induced most readily by markedly lowering the surface energy of the solid, leading to increased values of the equilibrium contact angle θ (based on the Young's relation[22]).

In our recent work,[19, 21] we discussed the synthesis and application of a new class of polyhedral oligomeric silsesquioxane (POSS) molecules, in which the silsesquioxane cage is surrounded by 1H,1H,2H,2H-heptadecafluorodecyl groups. These molecules are referred to as fluorodecyl POSS.[21] The high concentration of perfluorinated carbon atoms in the alkyl

chains leads to an extremely low solid surface energy for these molecules ($\gamma_{sv} \approx 10$ mN/m).[20] As a comparison, the surface energy of Teflon® is $\gamma_{sv} \approx 18$ mN/m.[36] To provide a conformal and flexible coating of fluorodecyl POSS molecules on any preformed substrate possessing re-entrant texture, we have developed a simple dip-coating procedure using the fluorodecyl POSS and a thermoplastic elastomeric binder (see experimental methods). After dip-coating, the equilibrium contact angle for rapeseed oil on a smooth glass slide increases to $\theta = 86°$; compared to $\theta \approx 0°$ on a clean uncoated glass slide (see supporting information for contact angle measurements with selected polar and non-polar liquids on a dip-coated glass slide). Dip-coating also increases the value of the robustness factor for rapeseed oil on a duck feather and a lotus leaf to $A^* \approx 4.2$ (assuming $R = 1$ μm, $D = 20$ μm) and $A^* \approx 26$ (assuming $R_{nub} = 2.5$ μm, $D_{nub} = 5$ μm) respectively (also see Fig. 2). Note that because the lotus leaf does not possess a cylindrical surface texture, the robustness factor A^* for the lotus leaf cannot be computed using Eq. 3 but requires a more complex expression.[20] As a result of the high values of the robustness factor, a dip-coated duck feather is able to support a composite interface even with hexadecane ($\gamma_{lv} = 27.5$ mN/m; $A^* = 3.3$) as shown in Fig. 1d.

In Fig. 3b we show an SEM micrograph highlighting the surface texture of a dip-coated lotus leaf. A comparison with the surface morphology of an uncoated lotus leaf (Fig. 3a) shows that all of the surface details, even features in the sub-micron range are preserved after dip-coating. The inset in Fig. 3b shows that the dip-coating process turns the surface of the leaf oleophobic, allowing it to support a robust composite interface with rapeseed oil and display large apparent contact angles ($\theta^* = 145°$).

Another general class of textured substrates possessing re-entrant curvature is commercial fabric.[37-40] Fig. 3c shows an electron micrograph of a commercial polyester fabric (Anticon 100 clean-room wipe). The inset in Fig. 3c shows that a droplet of hexadecane

completely wets the surface of the as-received polyester fabric. Fig. 3d shows the surface morphology of a polyester fabric dip-coated with fluorodecyl POSS. It is clear that all of the surface details of the polyester fabric are preserved after dip-coating. The inset in Fig. 3d shows the elemental mapping of fluorine on the dip-coated fabric surface using energy dispersive X-ray scattering (EDAXS). Dip-coating provides a conformal coating of fluorinated molecules on the fabric surface. The liquid repellency of the dip-coated fabric is highlighted in Fig. 3e which shows that this fabric is able to support a composite interface and display high apparent contact angles ($\theta^* \geq 140^o$) even with octane (γ_{lv} = 21.7 mN/m). Taking the geometry of the large fiber bundle as the dominant texture ($R_{bundle} = D_{bundle}$ = 150 μm, R_{fiber} = 5 μm, D_{fiber} = 10 μm, D^* = 6, θ = 60°), we obtain a value of the robustness factor A^* = 2.5 for octane. The measured contact angles on various dip-coated surfaces with selected polar and non-polar liquids are provided in the supporting information.

It should however be noted that when the equilibrium contact angle $\theta < 90°$, the composite interface is necessarily metastable,[4, 19, 20, 25, 41-43] i.e. it corresponds to a local minimum in the overall Gibbs free energy for the system, while the fully-wetted Wenzel state corresponds to the global minimum.[27]

To obtain even higher apparent contact angles with very low surface tension liquids, it is necessary to increase the value of the spacing ratio D^* (see Eq. 4). For fabrics, this can be readily achieved by equi-biaxial stretching such that the imposed strain is the same in both directions. Here strain is defined as $\varepsilon = (L - L_0)/L_0$, where L and L_0 represent the stretched and unstretched dimensions of the surface respectively. Stretching a fabric sample (such that the inter-fiber spacing D is increased for a fixed value of the fiber radius R) increases the spacing ratio to $D^*_{stretched} = D^*_{unstretched}\left(1+\varepsilon\right)$, leading to an increase in the value of the apparent contact angles. Based on the Cassie-Baxter relation[23] (Eq. 4), the apparent contact angles on the stretched fabric can then be computed as:

$$\cos\theta^*_{stretched} = -1 + \frac{1}{D^*_{stretched}}\left[\sin\theta + (\pi - \theta)\cos\theta\right] = -1 + \frac{1}{1+\varepsilon}(1 + \cos\theta^*_{unstretched}) \qquad (5)$$

However, as noted earlier, for a cylindrical geometry the two design parameters D^* and A^* are strongly coupled (see Eq. 3). As a result, increasing the inter-fiber spacing D causes more severe sagging of the liquid-air interface, leading to lower values of the robustness factor A^*. Thus, with increasing values of D^*, we expect to initially see an increase in the value of apparent contact angles θ^*, followed by a sudden transition to the Wenzel state once A^* decreases to a value close to unity.

The changes in the apparent advancing and receding contact angles for dodecane (γ_{lv} = 25.3 mN/m, $\theta = 70^o$) on a dip-coated polyester fabric, as a function of the applied strain are shown in **Fig. 4a**. As expected from Eq. 5, initially there is an increase in both the apparent advancing and receding contact angles with increasing strain due to the increasing fraction of trapped air underneath the liquid droplet. Fig. 4b shows the variation with applied strain in the values of both the robustness factor A^*, and the spacing ratio D^* for dodecane on the dip-coated fabric surface. Comparing the responses in Fig. 4a and 4b, we see a rapid transition from a composite or Cassie-Baxter interface to a wetted interface with both $\theta^*_{adv} = \theta^*_{rec} \approx 0°$ when $A^* \rightarrow 1$. Threshold values of A^* for the transition from the Cassie regime to the Wenzel regime were measured to be consistently close to unity (varying between A^* = 1.0 and A^* = 1.7) for various polar and non-polar liquids. Thus, biaxial stretching provides a simple mechanism for systematically adjusting the wetting properties of the dip-coated polyester fabric. To our knowledge, this is the first demonstration of tunable superoleophobicity on any surface.

An example of switchable oleophobicity of the fabric surface is shown in Fig. 4c. When a droplet of decane (γ_{lv} = 23.8 mN/m, $\theta = 60^o$) is placed on an unstretched (D^* = 6) dip-coated fabric, the relatively high value of the robustness factor (A^* = 2.8) enables the fabric to

support a composite interface with the decane droplet and thereby display high advancing apparent contact angles $\theta^* = 149^\circ \pm 2^\circ$ (see Fig. 4d). However, when the fabric is biaxially stretched to a strain of 30% (D^* = 7.8), the robustness factor is reduced to almost unity ($A^* \approx$ 1.4), and the fabric is fully wetted by the decane, with $\theta^*_{adv} \approx 0^\circ$ (see Fig. 4e).

When the strain on the fabric is released, the initial surface texture is restored. Returning to the original value of the inter-fiber spacing D leads once more to high values of the robustness factor A^*. This allows the fabric to once more support a composite Cassie-Baxter interface and display high apparent contact angles with a new droplet of decane placed at any location on its surface, except the spot where the initial liquid drop has been imbibed. The fabric is able to regenerate its oleophobic properties at the original wetted spot as well after a simple evaporative drying process. The data in Fig. 4c shows the apparent contact angles with decane at a single fixed location on the dip-coated polyester fabric. The first contact angle measurement is performed on the unstretched fabric. Next, the fabric is stretched until D^* increases to a value of 7.8 and correspondingly A^* decreases to a value of 1.4, leading to complete wetting. The strain is then removed and the fabric is placed in a vacuum oven to dry at 100°C for 20 minutes. This is followed by another contact angle measurement at the same location. Next, the fabric is stretched again and the cycle is repeated. It is clear from Fig. 4c that biaxial stretching enables the fabric to easily switch its wetting characteristics from perfectly oil-wetting to non-wetting, easily and reproducibly. Further, EDAXS elemental mapping (see supporting information) and microscopy on the dip-coated fabrics after the sixth cycle indicates that there is no apparent degradation in the fluorodecyl POSS coating after repeated stretching. Similar switchable wettability can also be achieved with ethanol (γ_{lv} = 22.1 mN/m), methanol (γ_{lv} = 22.7 mN/m) and dodecane (γ_{lv} = 25.3 mN/m) by stretching up to 20%, 30% and 60% strain respectively (see supporting information for data on switchable wettability with methanol).

From the definitions of the design parameters A^* and D^* in Eqs. 3 and 4, it is clear that for the same value of the spacing ratio D^*, different liquids possess different values of the robustness factor A^* due to differing values of surface tension, capillary length and equilibrium contact angle for each liquid on the fluorodecyl POSS-coated surface. Thus, while the dip-coated fabric may support a composite interface with a particular contacting liquid ($A^* >> 1$), another liquid with a lower surface tension may fully wet the fabric ($A^* \approx 1$). In addition, as we have shown in Fig. 4b, biaxial stretching of the fabric provides a simple mechanism to tune the robustness factor A^* and correspondingly adjust the conditions under which a liquid will wet and permeate into the fabric, or remain beaded up on the surface.

Fig. 5 highlights the strain-induced sequential wetting of a dip-coated polyester fabric with a series of different liquid drops by exploiting this sensitivity to the surface tension and equilibrium contact angle of the contacting liquid. The unstretched dip-coated fabric shown in Fig. 5a ($D^* = 6$) is able to support a composite interface with four different low surface tension alkanes; octane (γ_{lv} = 21.7 mN/m), decane (γ_{lv} = 23.8 mN/m), dodecane (γ_{lv} = 25.3 mN/m) and hexadecane (γ_{lv} = 27.5 mN/m). Starting from this initial state, we continuously increase the applied strain on the fabric. At a strain of 15% the spacing ratio reaches a value of $D^* = 6.9$, and the lowest surface tension oil (octane, $A^*_{octane} \approx 1.7$) transitions to a fully wetted Wenzel state (Fig. 5b), while the other three liquids maintain a Cassie-Baxter composite interface with the dip-coated fabric. Thus, the stretched fabric can demonstrate remarkably different wetting properties with liquids having a surface tension difference of only $\Delta\gamma_{lv} \sim 2$ mN/m between them. Additional strain increases the spacing ratio further; once it reaches a value of $D^* = 7.8$, the decane droplet ($A^*_{decane} \approx 1.4$) wets the fabric surface (Fig. 5c), while dodecane and hexadecane still maintain a non-wetting composite interface. Further stretching of the fabric (until $D^* = 9.6$) causes even the dodecane drop ($A^*_{dodecane} \approx 1.0$) to be imbibed into the fabric (Fig. 5d).

In conclusion, in this work we have developed a simple and benign dip-coating process that enables us to provide a flexible and conformal coating of extremely low surface energy fluorodecyl POSS molecules on any surface, including those that inherently possess re-entrant texture, such as duck feathers, lotus leaves or commercially available fabrics. The synergistic effect of roughness, re-entrant topography of the substrate, and the low surface energy of fluorodecyl POSS molecules, enables the dip-coated texture to support a composite interface even with very low surface tension liquids. We have also used two design parameters D^* and A^* to provide an *a priori* estimate of both the apparent contact angles as well as the robustness of the composite Cassie-Baxter interface. The design framework outlined in this paper enables us to identify and develop suitably textured surfaces which can have their surface wettability characteristics systematically adjusted. By combining this understanding with a dip-coating process that provides a conformal and flexible fluorinated coating, we can reversibly switch the wettability behavior of fabric surfaces between super-wetting and super-repellent with a wide range of polar and non-polar liquids using simple mechanical deformation. Biaxial stretching of a dip-coated, commercial polyester fabric can cause an appreciable increase in both the apparent advancing and receding contact angles as predicted by changes in the spacing ratio D^*. As a result of the strong coupling between the two design parameters A^* and D^* for a typical woven fibrous geometry, stretching commercial fabrics can lead to a dramatic reduction in the robustness of the composite interface that is supported with a given contacting liquid. Indeed, beyond a critical strain (at which the robustness A^* decreases to values close to unity), the contacting liquid spontaneously penetrates the fabric texture, leading to near zero contact angles. However, because of the conformal and flexible characteristics of the fluorodecyl POSS coating, mechanical unloading and drying of the fabric enables the super-repellency of the sample to be regained repeatedly.

Experimental Section

Dip-coating: For the dip-coating process, we first prepare a solution of 50 wt% fluorodecyl POSS and Tecnoflon® (BR9151) in Asahiklin AK-225 (Asahi glass company) at an overall solid concentration of 10 mg/ml. Tecnoflon is a commercial fluoro-elastomer manufactured by Solvay-Solexis. The use of Tecnoflon as a polymeric binder prevents the crystallization of fluorodecyl POSS, and yields a more conformal and elastomeric coating. Next, the substrate to be dip-coated is immersed in the fluorodecyl POSS-Tecnoflon solution. After 5 minutes, the substrate is removed from the solution and placed to dry in a vacuum oven for 30 minutes at a temperature of 60^{o}C.

Biaxial Stretching: The fabric stretching experiments were carried out using a custom built biaxial stretcher. Multiple markings were made on the fabric surface, with an inter-marking separation of 5 mm on the unstretched fabric. Next, as the fabric was stretched, we measured the separation between the markings to provide an accurate measurement of strain.

Contact angle measurements: The contact angles for various liquids were measured using a contact angle goniometer, VCA2000 (AST Inc.). The advancing contact angle was measured by advancing a small volume of the probing liquid (typically 2-4 μl) on to the surface, using a syringe. The receding contact angle was measured by slowly removing the probing liquid from a drop already on the surface. For each sample a minimum of four different readings were recorded. Typical error in measurements was ~ 2°.

Received:
Revised:
Published online:

References:

[1] W. Chen, A. Y. Fadeev, M. C. Hsieh, D. Oner, J. Youngblood, T. J. McCarthy, *Langmuir* **1999**, *15*, 3395.
[2] C. Dorrer, J. Ruhe, *Adv. Mater.* **2008**, *20*, 159.
[3] X. J. Feng, L. Jiang, *Adv. Mater.* **2006**, *18*, 3063.
[4] S. Herminghaus, *Europhys. Lett.* **2000**, *52*, 165.
[5] K. K. S. Lau, J. Bico, K. B. K. Teo, M. Chhowalla, G. A. J. Amaratunga, W. I. Milne, G. H. McKinley, K. K. Gleason, *Nano Lett.* **2003**, *3*, 1701.
[6] A. Nakajima, K. Hashimoto, T. Watanabe, *Monatshefte Fur Chemie* **2001**, *132*, 31.
[7] D. Quéré, *Rep. Prog. Phys.* **2005**, *68*, 2495.
[8] N. J. Shirtcliffe, G. Mchale, M. I. Newton, C. C. Perry, P. Roach, *Chem. Comm.* **2005**, 3135.
[9] L. Zhai, M. C. Berg, F. C. Cebeci, Y. Kim, J. M. Milwid, M. F. Rubner, R. E. Cohen, *Nano Lett.* **2006**, *6*, 1213.
[10] N. Verplanck, Y. Coffinier, V. Thomy, R. Boukherroub, *Nano. Res. Lett.* **2007**, *2*, 577.
[11] R. Furstner, W. Barthlott, C. Neinhuis, P. Walzel, *Langmuir* **2005**, *21*, 956.
[12] L. Feng, Z. Y. Zhang, Z. H. Mai, Y. M. Ma, B. Q. Liu, L. Jiang, D. B. Zhu, *Angew. Chem. Int. Ed.* **2004**, *43*, 2012.
[13] F. C. Cebeci, Z. Z. Wu, L. Zhai, R. E. Cohen, M. F. Rubner, *Langmuir* **2006**, *22*, 2856.
[14] J. Lahann, S. Mitragotri, T. N. Tran, H. Kaido, J. Sundaram, I. S. Choi, S. Hoffer, G. A. Somorjai, R. Langer, *Science* **2003**, *299*, 371.
[15] A. Ahuja, J. A. Taylor, V. Lifton, A. A. Sidorenko, T. R. Salamon, E. J. Lobaton, P. Kolodner, T. N. Krupenkin, *Langmuir* **2008**, *24*, 9.

[16] T. N. Krupenkin, J. A. Taylor, E. N. Wang, P. Kolodner, M. Hodes, T. R. Salamon, *Langmuir* **2007**, *23*, 9128.
[17] J. L. Zhang, X. Y. Lu, W. H. Huang, Y. C. Han, *Macro. Rapid Comm.* **2005**, *26*, 477.
[18] J. Y. Chung, J. P. Youngblood, C. M. Stafford, *Soft Matter* **2007**, *3*, 1163.
[19] A. Tuteja, W. Choi, M. L. Ma, J. M. Mabry, S. A. Mazzella, G. C. Rutledge, G. H. McKinley, R. E. Cohen, *Science* **2007**, *318*, 1618.
[20] A. Tuteja, W. Choi, J. M. Mabry, G. H. McKinley, R. E. Cohen, *Proc. Nat. Acad. Sci.* **2008**, *105*, 18200.
[21] J. M. Mabry, A. Vij, S. T. Iacono, B. D. Viers, *Angew. Chem. Int. Ed.* **2008**, *47*, 4137.
[22] T. Young, *Philos. Trans. R. Soc. London* **1805**, *95*, 65.
[23] A. B. D. Cassie, S. Baxter, *Trans. Faraday Soc.* **1944**, *40*, 546.
[24] A. Marmur, *Langmuir* **2003**, *19*, 8343.
[25] M. Nosonovsky, *Langmuir* **2007**, *23*, 3157.
[26] Nosonovsky[25] recently derived another important criterion for the creation of a local minimum in free energy, and thus for the creation of a stable heterogeneous interface: $dA_{sl}d\theta < 0$, where dA_{sl} is the change in solid-liquid contact area with the advancing or receding of the liquid, and $d\theta$ is the change in local contact angle. This criterion also emphasizes the importance of re-entrant surfaces.
[27] A. Tuteja, W. Choi, G. H. McKinley, R. E. Cohen, M. F. Rubner, *MRS bull.* **2008**, *33*, 752.
[28] A. Marmur, *Langmuir* **2008**, *24*, 7573.
[29] B. He, N. A. Patankar, J. Lee, *Langmuir* **2003**, *19*, 4999.
[30] G. McHale, N. J. Shirtcliffe, M. I. Newton, *Langmuir* **2004**, *20*, 10146.
[31] D. Quéré, *Phys. A-Stat. Mech. and Appl.* **2002**, *313*, 32.
[32] D. Quéré, M. Reyssat, *Phil. Trans. Royal Soc. A-Math. Phys. Eng. Sci.* **2008**, *366*, 1539.
[33] R. N. Wenzel, *Ind. & Eng. Chem.* **1936**, *28*, 988.
[34] L. C. Gao, T. J. McCarthy, *Langmuir* **2006**, *22*, 5998.
[35] N. J. Shirtcliffe, G. McHale, M. I. Newton, G. Chabrol, C. C. Perry, *Adv. Mater.* **2004**, *16*, 1929.
[36] W. A. Zisman, *Relation of the equilibrium contact angle to liquid and solid construction. In Contact Angle, Wettability and Adhesion, ACS Advances in Chemistry Series.*, Vol. 43, American Chemical Society, Washington, DC. **1964**.
[37] S. A. Brewer, C. R. Willis, *Appl. Surf. Sci.* **2008**, *254*, 6450.
[38] H. F. Hoefnagels, D. Wu, G. de With, W. Ming, *Langmuir* **2007**, *23*, 13158.
[39] S. Michielsen, H. J. Lee, *Langmuir* **2007**, *23*, 6004.
[40] K. Ramaratnam, V. Tsyalkovsky, V. Klep, I. Luzinov, *Chem. Comm.* **2007**, 4510.
[41] L. L. Cao, H. H. Hu, D. Gao, *Langmuir* **2007**, *23*, 4310.
[42] J. L. Liu, X. Q. Feng, G. F. Wang, S. W. Yu, *J. Phys Cond. Mat.* **2007**, *19*.
[43] K. Kurogi, H. Yan, K. Tsujii, *Coll. & Surfaces A-Physicochem. and Engg. Asp.* **2008**, *317*, 592.

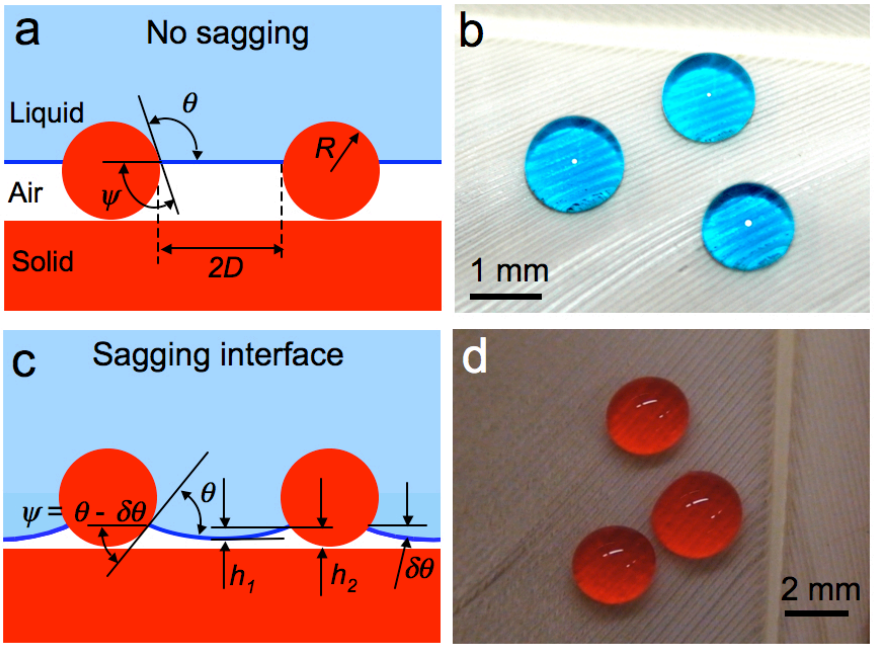

Figure 1. (a) A schematic diagram illustrating the expected liquid–air interface on a textured surface with an equilibrium contact angle $\theta \sim 100^{o}$. In this schematic, the sagging of the liquid-air interface caused by any pressure differential across the interface, is ignored. (b) Droplets of water (colored with methylene blue) on a duck feather. (c) A schematic illustrating the putative liquid-air interface on a textured surface with an equilibrium contact angle $\theta \sim 70^{o}$. The schematic also illustrates the various parameters used to characterize the sagging of the liquid-air interface. (d) Droplets of hexadecane (γ_{lv} = 27.5 mN/m, colored with Oil Red O) on a dip-coated duck feather. A reflective surface is visible under the droplets in the image, indicating the presence of microscopic pockets of air due to the formation of a composite interface.

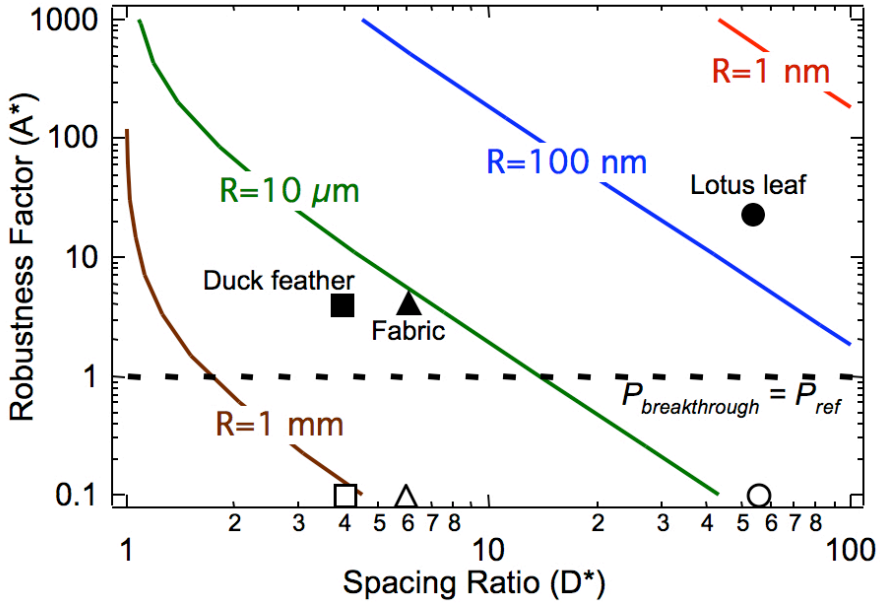

Figure 2. Computed robustness parameter A^* for rapeseed oil (γ_{lv} = 35.7 mN/m, θ = 86°) on a surface texture composed of periodic cylindrical features, as a function of the spacing ratio $D^* = (R + D)/R$. Values of the robustness parameter for various uncoated (unfilled symbols) and dip-coated surfaces (filled symbols) against rapeseed oil are also shown. A^* calculations for the non-coated surfaces are based on the assumption that θ = 20°.

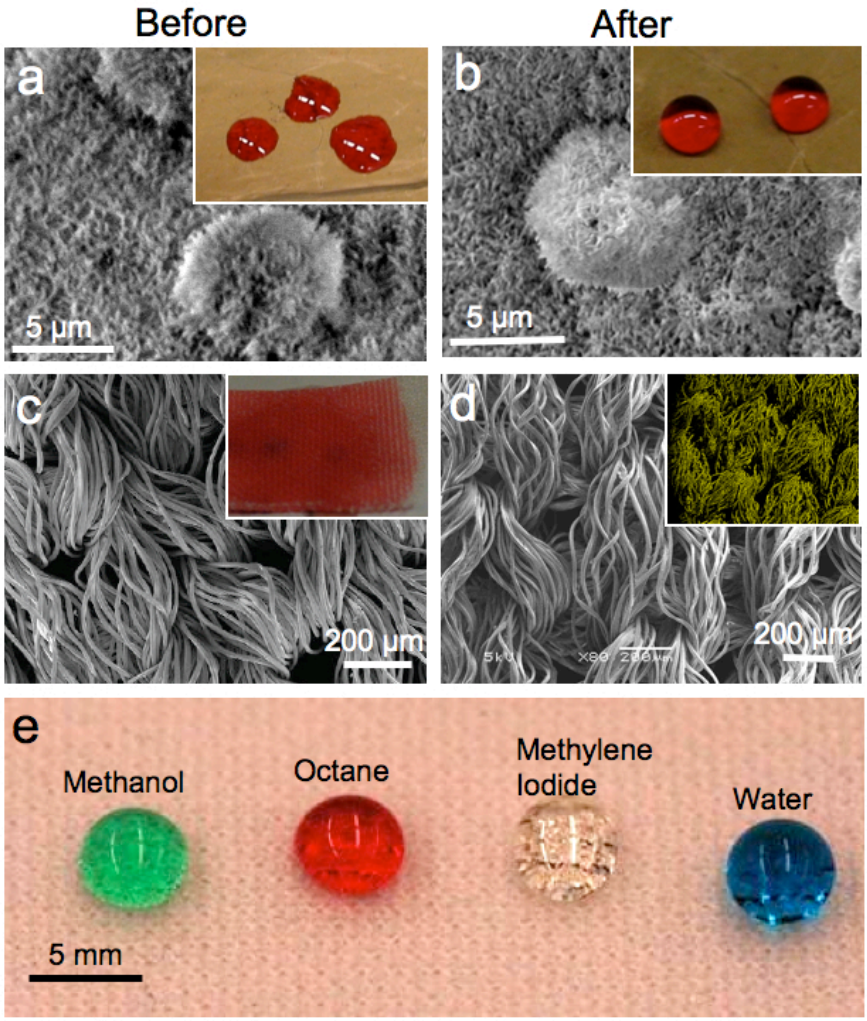

Figure 3. (a) A scanning electron microscope (SEM) image of a lotus leaf illustrating its surface texture. The inset shows that droplets of rapeseed oil easily wet the surface of a lotus leaf ($\theta^* \approx 10°$). (b) An SEM image of a lotus leaf surface after the dip coating process. The inset shows that the dip-coated leaf is significantly more repellent to rapeseed oil ($\theta^* \approx 145°$) (c) An SEM image of the polyester fabric. In spite of the presence of re-entrant curvature, hexadecane can readily wet the fabric surface (inset). (d) An SEM image of the dip-coated polyester fabric. The inset shows the elemental mapping of fluorine obtained using energy dispersive X-ray scattering (EDAXS) (e) Super-repellency of a dip-coated polyester fabric against various polar and non-polar liquids.

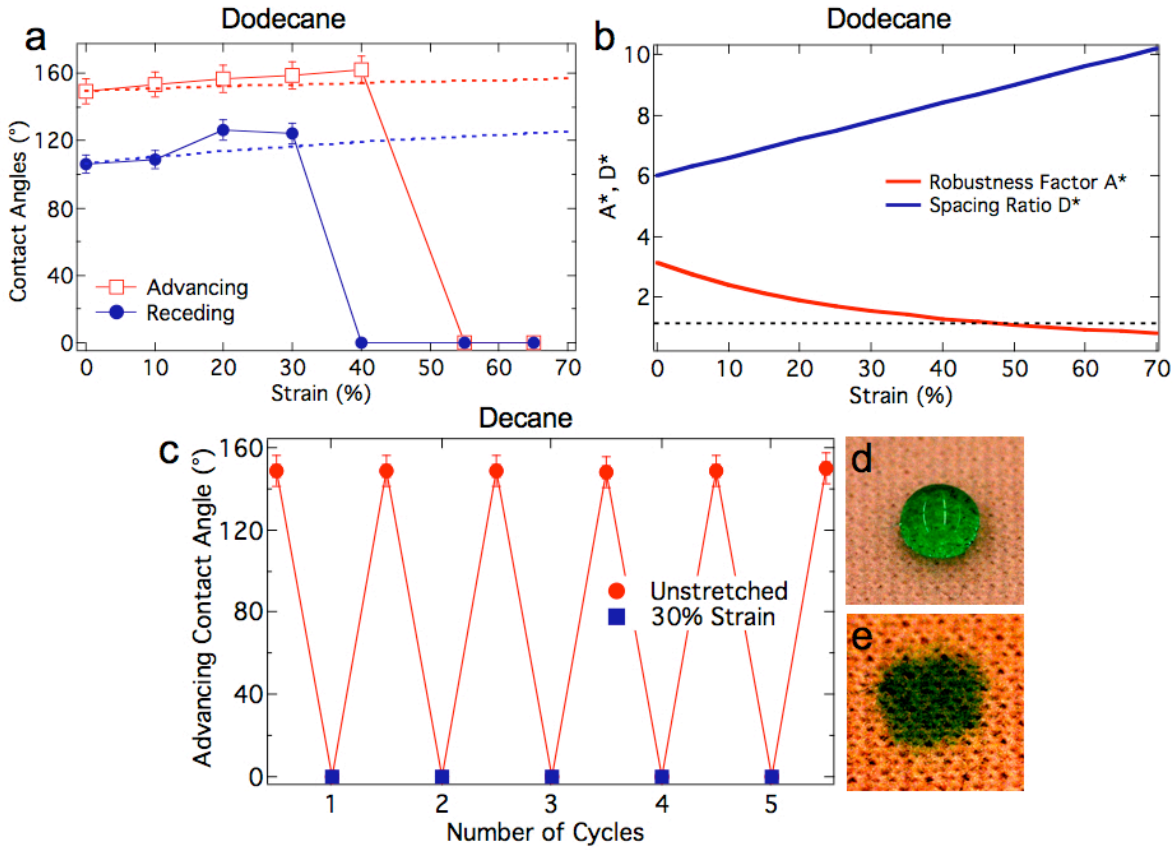

Figure 4. (a) The apparent advancing (red squares) and receding (blue dots) contact angles for dodecane (γ_{lv} = 25.3 mN/m) on a dip-coated polyester fabric, as a function of the applied bi-axial strain. The dashed red and blue lines are the apparent contact angles predicted by Eq. 5. (b) Predictions for A^* (red line) and D^* (blue line) as a function of the imposed bi-axial strain on the fabric. (c) Switchable oleophobicity of the dip-coated fabric with decane (γ_{lv} = 23.8 mN/m). (d) and (e) Decane droplets on, respectively, an unstretched and stretched (30% bi-axial strain) dip-coated polyester fabric.

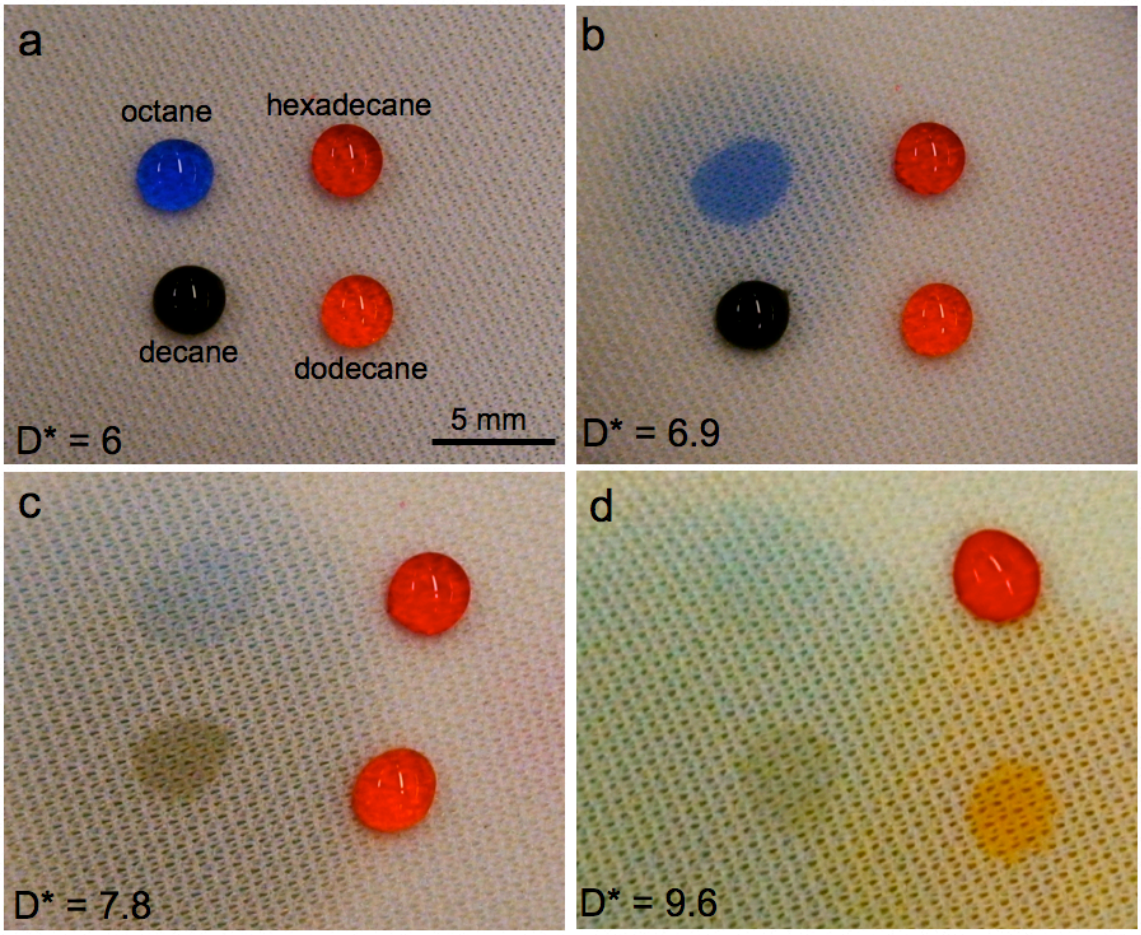

Figure 5. Sequential wetting of four alkane droplets on a dip-coated polyester fabric. (a) Super-repellency of the unstretched, dip-coated, fabric against octane (γ_{lv} = 21.7 mN/m, θ = 55^o), decane (γ_{lv} = 23.8 mN/m, θ = 60^o), dodecane(γ_{lv} = 25.3 mN/m, θ = 70^o) and hexadecane (γ_{lv} = 27.8 mN/m, θ = 78^o). (b) At 15% strain, the octane droplet transitions to the Wenzel regime with A^*_{octane} = 1.7. (c) At 30% strain, the decane droplet transitions to the Wenzel regime with A^*_{decane} = 1.4. (d) At 60% strain, the dodecane droplet transitions to the Wenzel regime with $A^*_{dodecane}$ = 1.0. The hexadecane droplet does not transition into the Wenzel regime until the woven fabric starts to tear apart at ~70% strain.

Table of contents entry.

In the present work we report a simple 'dip-coating' process that imbues oleophobicity to various surfaces that inherently possess re-entrant texture, such as commercially available fabrics, as shown in the following figure. We also show that such dip-coated fabric surfaces exhibit, reversible, deformation-dependent, tunable wettability, including the capacity to switch their surface wetting properties (between super-repellent and super-wetting) against a wide range of polar and non-polar liquids.

Keywords: Superoleophobic, Super-wetting, Super-repellency, Dip-coating, Tunable wettability

Authors: Wonjae Choi,[**] Anish Tuteja,[**] Shreerang Chhatre, Joseph M. Mabry, Robert E. Cohen* and Gareth H. McKinley*

[**]: these authors contributed equally to this work

*: Corresponding authors
Prof. Gareth H. McKinley (gareth@mit.edu)
Prof. Robert E. Cohen (recohen@mit.edu)

Title: Fabrics with Tunable Oleophobicity.

Table of contents figure:

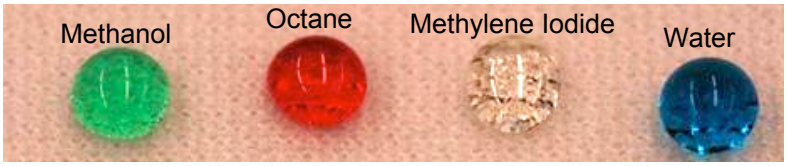

Submitted to ADVANCED MATERIALS

Supporting Information - Fabrics with Tunable Oleophobicity

By *Wonjae Choi*,[1**] *Anish Tuteja*,[2**] *Shreerang Chhatre*,[2] *Joseph M. Mabry*,[3] *Robert E. Cohen*[2]* and *Gareth H. McKinley*[1]*

([**]: these authors contributed equally to this work)

Table S1. A compilation of apparent advancing contact angles for selected polar and non-polar liquids obtained on various dip-coated surfaces. The dip-coating solution is composed of 50 wt% fluorodecyl POSS and Tecnoflon® (BR9151) in Asahiklin AK-225 at an overall solid concentration of 10 mg/ml. The equilibrium contact angle $\theta_{dip\text{-}coated}$ refers to the equilibrium contact angle measured on a glass slide dip-coated in the same solution as above. Contact angles denoted ≈0˚ indicate that the metastable surface obtained following dipcoating was not sufficiently robust to support a 2 µl droplet for a fluid of that value of surface tension, and that the liquid droplet was imbibed into the re-entrant texture of the surface.

Liquid	γ_{lv} (mN/m)	$\theta_{dip\text{-}coated}$	θ^* (advancing)		
			Lotus leaf	Duck feather	Fabric
Water	72.1	120°	163°	151°	158°
Rapeseed Oil	35.7	86°	145°	138°	152°
Methanol	22.7	57°	109°	≈0°	148°
Octane	21.7	55°	≈0°	≈0°	140°

Section 1. The microscopic texture of a duck feather.

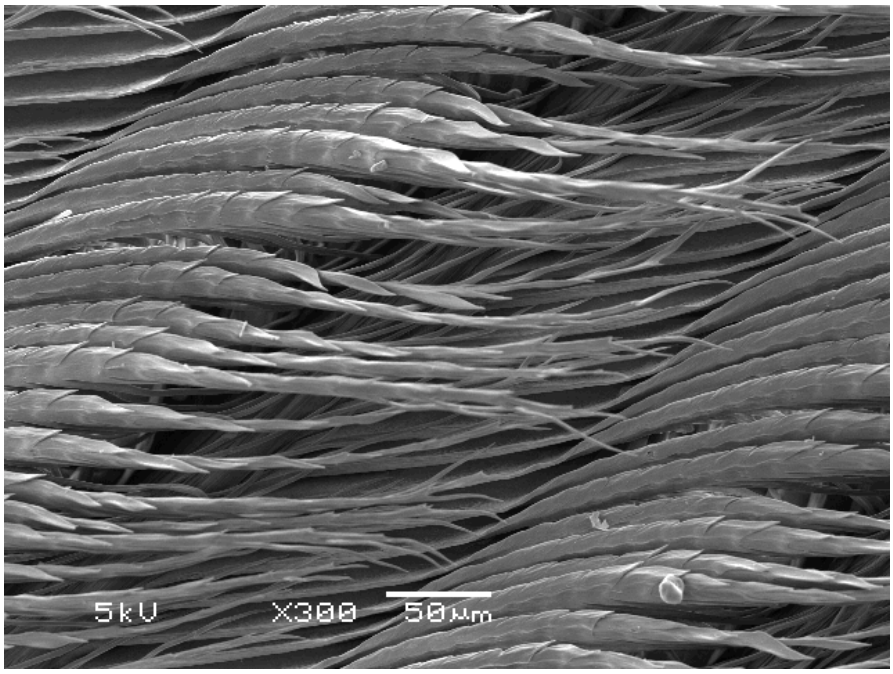

Figure S1. An SEM image illustrating the surface topography of a duck feather.

Section 2. The robustness factor A^*.

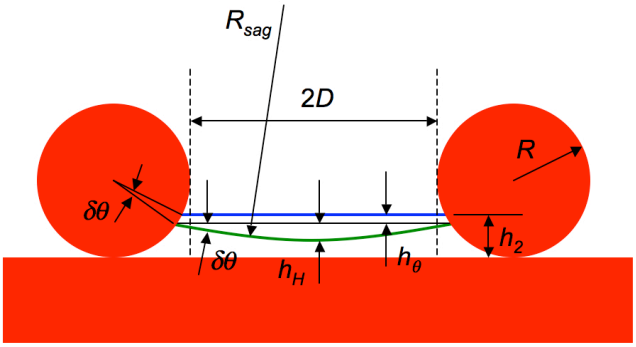

Figure S2. A schematic diagram illustrating the sagging of the liquid-vapor interface on the application of an external pressure difference across the free surface. On the application of a pressure differential the original liquid-air interface (shown in blue in Fig. S2) sags downward to a new position (shown in green in Fig. S2) by the amount equal to h_H, but the contact line between the interface and the solid moves downward as well by h_θ.

In our previous work,[1] we developed the dimensionless design parameter H^* (called the robustness height), to provide a dimensionless measure of the pressure (P_H) required to force the sagging height, h_H, for the liquid-vapor interface to reach the maximum pore depth, h_2 (see Fig. S2). In evaluating H^*, we compare P_H to a reference pressure $P_{ref} = 2\gamma_{lv} / \ell_{cap}$, where $\ell_{cap} = \sqrt{\gamma_{lv} / \rho g}$ is the capillary length of the fluid, ρ is the liquid density, and g is the acceleration due to gravity. As defined, P_{ref} is close to the minimum pressure difference across the composite solid-liquid-air interface for millimetric sized droplets or larger puddles on extremely non-wetting, textured surfaces.[1] For a predominantly cylindrical texture, such as the duck feathers or the fabric surfaces, the robustness height is given as[1]:

$$H^* = \frac{P_H}{P_{ref}} = \frac{\left(1-\cos\theta\right) R\ell_{cap}}{D^2} \tag{S1}$$

Similarly, the design parameter T^* (called the robustness angle) provides a dimensionless measure of the pressure differential (P_θ) required to force a sagging angle of $\delta\theta = \theta - \psi_{min}$. Here ψ_{min} is the minimum value of the local texture angle. For a cylindrical geometry, recognizing that $\psi_{min} = 0°$, the robustness angle T^* takes the form[1]:

$$T^* = \frac{P_\theta}{P_{ref}} = \frac{\ell_{cap} \sin\theta}{2D} \tag{S2}$$

The application of external pressure causes a simultaneous increase in both the sagging height h_1 and the sagging angle $\delta\theta$. Thus, we showed in our previous work[1] that the robustness of any composite interface is proportional to a combined robustness factor A^* of the form:

$$\frac{1}{A^*} = \frac{C_1}{H^*} + \frac{C_2}{T^*} \tag{S3}$$

where the coefficients C_1 and C_2 are functions of the specifics of the surface geometry.

For a texture that is dominated by periodic cylindrical features, such as the duck feathers or the fabric surfaces considered in the present work, the robustness measure A^* can be calculated to be[1]:

$$\frac{1}{A^*} = \frac{1}{H^*} + \frac{\sin^2\theta}{\left(1-\cos\theta\right)T^*} \tag{S4}$$

By substituting for the design parameters H^* and T^*, we obtain the following compact expression for the robustness factor A^*:

$$A^* = \frac{P_{breakthrough}}{P_{ref}} = \frac{R\ell_{cap}}{D^2}\frac{\left(1-\cos\theta\right)}{\left(1+2(R/D)\sin\theta\right)} \tag{S5}$$

Here $P_{breakthrough}$ is the breakthrough pressure, defined as the pressure differential required to disrupt a composite interface and force a transition between the Cassie and Wenzel states. For our surfaces, recognizing that $\frac{\sin^2\theta}{\left(1-\cos\theta\right)} \sim$ O(1) (when $\theta < 90°$, provided $\theta \neq 0$), we can re-write Eq. S4 in the approximate functional form:

$$\frac{1}{A^*} \approx \frac{1}{H^*} + \frac{1}{T^*} \tag{S6}$$

For the cylindrical textures in the present work this leads to the following approximate form for the robustness factor A^*:

$$A^* = \frac{P_{breakthrough}}{P_{ref}} = \left(\frac{R\ell_{cap}}{D^2}\right)\frac{\sin\theta(1-\cos\theta)}{\sin\theta+2(R/D)(1-\cos\theta)} \tag{S7}$$

Fig. S3 shows the comparison between the exact form of A^* (Eq. S5) and the approximate form for A^* (Eq. S7) over the range $0° < \theta < 180°$. It can be seen that there is almost no difference in the values obtained from the two relations in the range $0° < \theta < 90°$. It is also clear from the figure that for values of the equilibrium contact angle $\theta >> 90°$, Eq. S5 must be used to compute A^* accurately. However, the maximum value for the equilibrium contact angles obtained on smooth surfaces is in the range of $\theta \approx 110 - 120°$, even for water on a perfluorinated surface. For an equilibrium contact angle of $\theta = 110°$, the difference between the values of the robustness factor A^*, obtained using Eq. S5 and Eq. S7 is less than 25%. For most organic liquids, such as those used in this work, $\theta < 90°$, and either Eq. S5 or Eq. S7 may be used to compute A^*. In the present work, we use Eq. S5 throughout to compute the values of the robustness factor A^*.

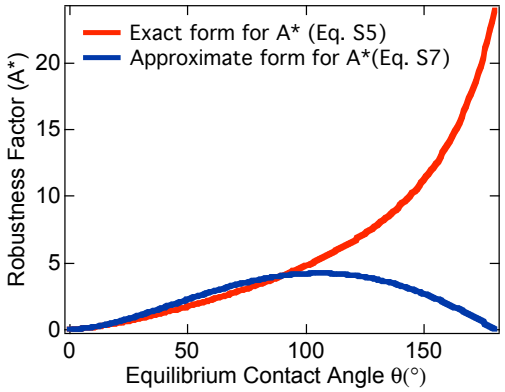

Figure S3. A comparison between the values of the robustness factor A^* obtained using Eq. S5 and Eq. S7 for octane (ℓ_{cap} = 1.8 mm) on the polyester fabric surface ($R_{bundle} = D_{bundle}$ = 150 μm).

Section 3. Derivation of D^* and A^* for surfaces with non-uniform structure.

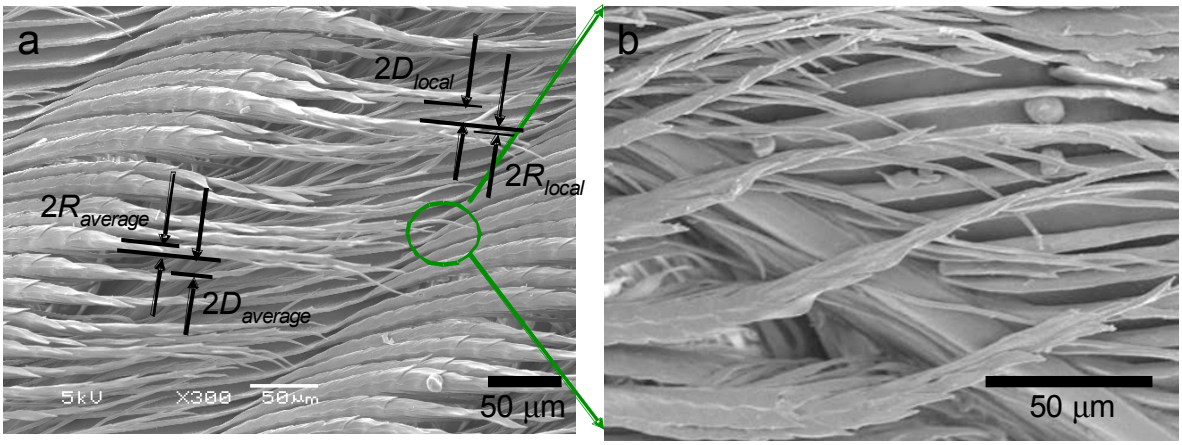

Figure S4. (a) An SEM image illustrating the non-uniform texture of a duck feather. The image clearly shows the variation in the surface texture parameters, R_{local} and D_{local}, along the length of a barbule. (b) A higher magnification SEM image showing the ends of a duck feather barbule.

Although local variation in the surface texture parameters, R and D, can affect the degree of local pinning or droplet anisotropy,[2] the Cassie-Baxter relation (Eq. 1) and the corresponding dimensionless measure D^* (Eq. 4) are derived to provide a general estimate of the apparent contact angles. Thus, for the duck feathers (Fig. S4-a), the average value of the barbule radius ($R_{average}$) and the barbule spacing ($D_{average}$) may be used for calculating values of D^*. However, the robustness factor (A^*) cannot be evaluated based on the average value of the barbule radius and spacing, as the transition from a composite to a wetted interface always occurs at the least robust location on the surface (see the region marked with a green circle in

Fig. S4-a). Once one particular area on the feather surface is wetted by the contacting liquid, the wicking spontaneously spreads along the barbules and the composite interface transitions completely to a wetted interface. To estimate the robustness of a composite interface on such surfaces, we need to use those values of the local texture parameters (R_{local}, D_{local}; see Fig. S4-a) that yield the lowest values for the robustness factor (A^*). For example, the average radius and inter-spacing between barbules is 5 μm and 15 μm respectively, which yields a value of the spacing ratio $D^* = 4$, and the robustness factor $A^* = 25$ is overestimated. On the other hand, using the local radius (R_{local} = 1 μm) and local inter-barbule spacing (D_{local} = 20 μm) between the tips of the barbules, yields a value of $A^* = 4$ for the robustness factor. Another example of a surface possessing variable texture parameters R, D along its surface is the polyester fabric which possesses multiple scales of roughness (see supporting information section 4) with $R_{bundle} = D_{bundle}$ = 150 μm, R_{fiber} = 5 μm and D_{fiber} = 7.5 μm. For the polyester fabric surface, the robustness parameter A^* should be derived using R_{bundle} and D_{bundle} as these would yield the lowest value for the robustness of the composite interface. Similarly the lotus leaf possesses multiple scales of roughness with R_{nub} = 2.5 μm, D_{nub} = 5 μm, R_{fiber} = 0.1 ~ 0.2 μm and D_{fiber} = 0.1 ~ 0.2 μm. For the lotus leaf surface, the robustness parameter A^* should be derived using R_{nub} and D_{nub} as these would yield the lowest value for the robustness of the composite interface.

Section 4. Derivation of spacing ratio D^* for a fabric surface.

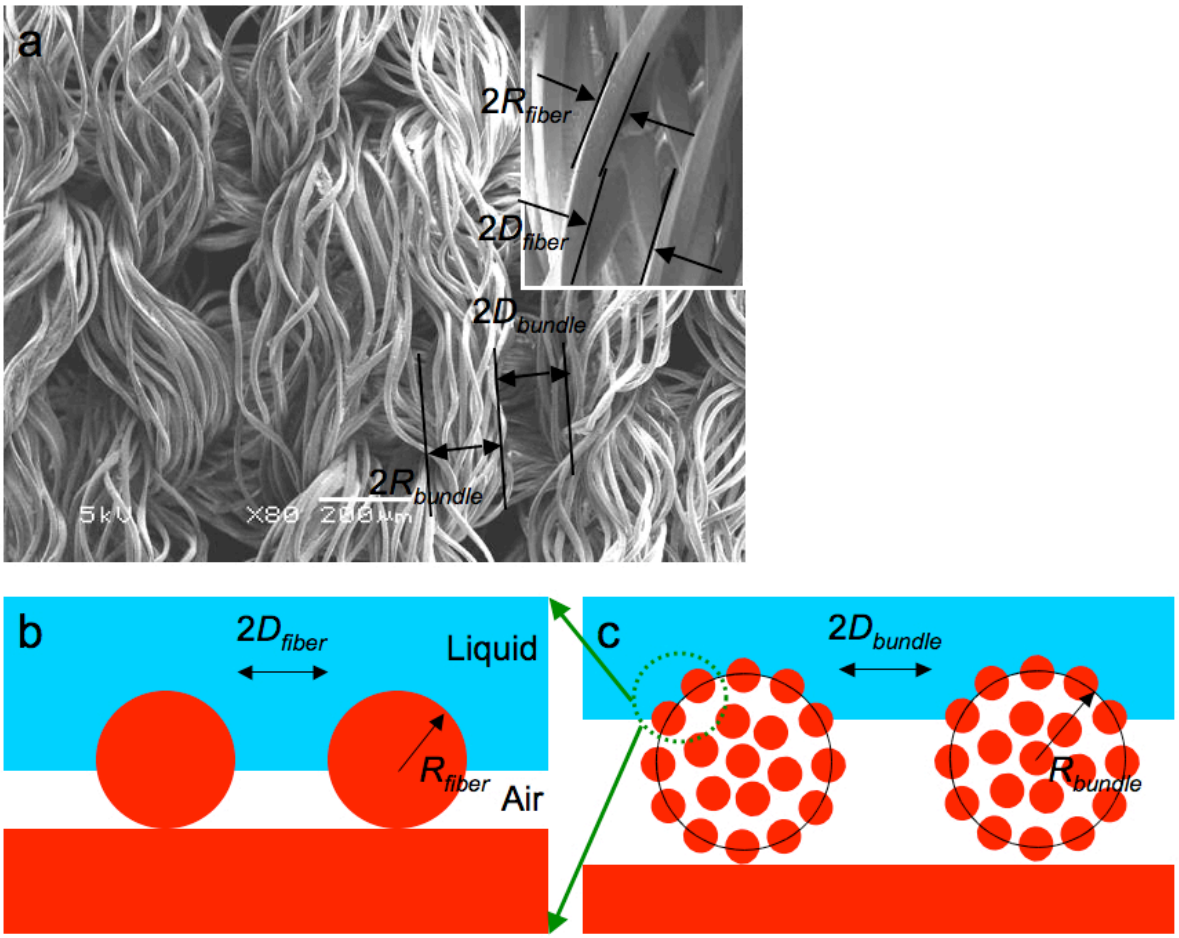

Figure S5. (a) An SEM image illustrating the multiple scales of roughness and corresponding values for the bundle radius (R_{bundle}) and the inter-bundle spacing (D_{bundle}) for a fabric surface. (b) A schematic representation of a composite interface on an array of fibers, where the classic Cassie-Baxter relation can be applied without modification to estimate apparent contact angles. (c) A composite interface on an array of fiber bundles. To estimate the apparent contact angles on this surface, a recursive form of Cassie-Baxter relation should be applied.

The surface of the polyester fabric used in our work has multiple scales of roughness or porosity.[3, 4] As is clear from Fig. S5-a, the fabric surface is composed of multiple fiber bundles, with an inter-bundle spacing of $2D_{bundle}$. Each of these fiber bundles, in turn, is also porous with finite inter-fiber spacing ($2D_{fiber}$; see inset of Fig. S5-a). Indeed, various other synthetic and natural surfaces, such as the lotus leaf or duck feathers also possess multiple scales of roughness.[5, 6] Herminghaus first noted that to compute the apparent contact angles on such surfaces, the Cassie-Baxter equation should be used recursively.[7] In a similar way, to

compute the D^* values for surfaces with multiple scales of roughness, such as the polyester fabric, we can define D^*_{fabric} as

$$D^*_{fabric} = \frac{(R_{fiber} + D_{fiber})}{R_{fiber}} \times \frac{(R_{bundle} + D_{bundle})}{R_{bundle}} = D^*_{fiber} \times D^*_{bundle} \quad \text{(S8)}$$

For the polyester fabric used in our work, $R_{bundle} = D_{bundle} = 150$ μm, $R_{fiber} = 5$ μm and $D_{fiber} = 10$ μm. Thus $D^*_{fabric} = D^*_{fiber} \times D^*_{bundle} = 6$.

Section 5. Durability of a dip-coated polyester fabric surface.

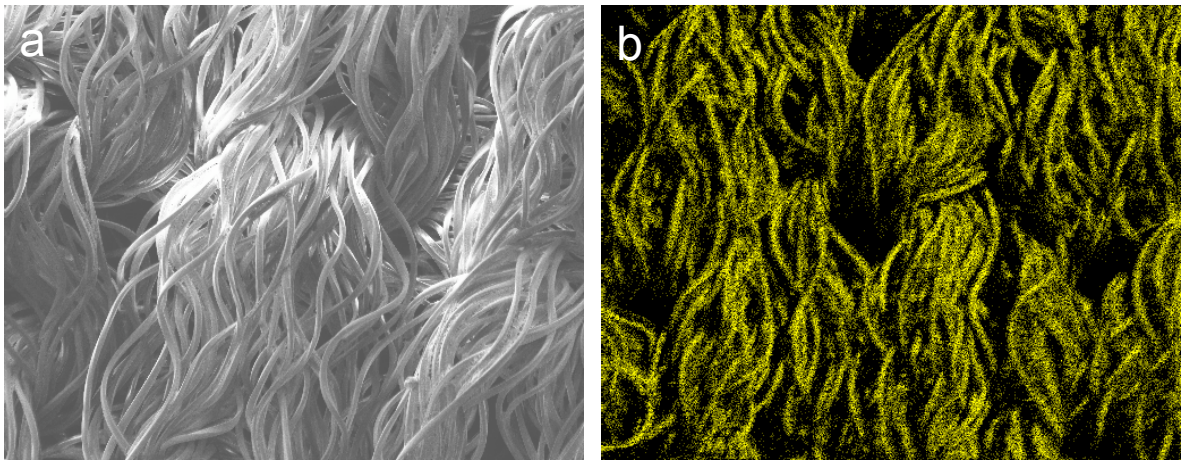

Figure S6. (a) An SEM image of the fabric surface after the 6th cycle of the stretching test described in Fig. 4c. (b) EDAXS elemental mapping of fluorine on the same fabric.

Section 6. Switchable wettability with methanol

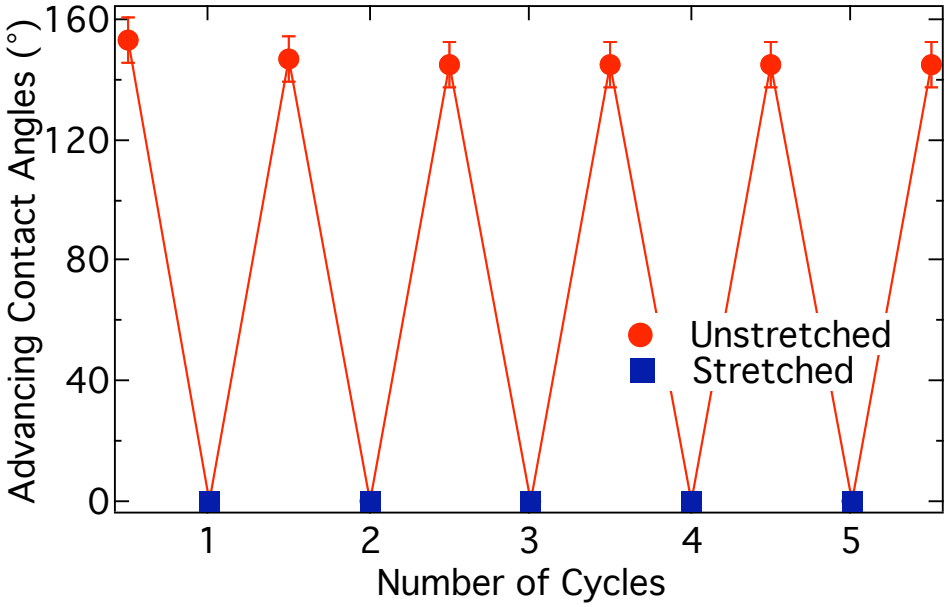

Figure S7. Switchable wettability of the dip-coated fabric with methanol (γ_{lv} = 22.7 mN/m, θ = 57°) obtained through the biaxial stretching (D^* = 7.8, A^* = 1.2) and unloading (D^* = 6, A^* = 2.5) of the fabric. The imposed loading in each cycle results in a biaxial strain of 30%. The droplet volume for each measurement is 2 µl. Also, all contact angle measurements are performed on the same location, as the fabric is able to regenerate its oleophobic properties at the original wetted spot after a simple evaporative drying process, as discussed in detail in the main manuscript.

References.

[1] A. Tuteja, W. Choi, J. M. Mabry, G. H. McKinley, R. E. Cohen, *Proc. Nat. Acad. Sci.* **2008**, *105*, 18200.
[2] C. W. Extrand, *Langmuir* **2002**, *18*, 7991.
[3] H. F. Hoefnagels, D. Wu, G. de With, W. Ming, *Langmuir* **2007**, *23*, 13158.
[4] L. C. Gao, T. J. McCarthy, *Langmuir* **2006**, *22*, 5998.
[5] R. Furstner, W. Barthlott, C. Neinhuis, P. Walzel, *Langmuir* **2005**, *21*, 956.
[6] X. J. Feng, L. Jiang, *Adv. Mater.* **2006**, *18*, 3063.
[7] S. Herminghaus, *Europhys. Lett.* **2000**, *52*, 165.